

# Ubiquitous variability of X-ray absorbing column densities in Seyfert 2 Galaxies

G. Risaliti<sup>1,2,3</sup>, M. Elvis<sup>1</sup>, F. Nicastro<sup>1</sup>

grisaliti@cfa.harvard.edu

## ABSTRACT

We present a study of the variations in the absorbing column density of 25 X-ray defined Seyfert 2 galaxies, as inferred from hard X-ray observations, on timescales from months to several years. We show that a significant variation of  $N_H$  (from 20% to 80%) is observed in almost all (22/25) the sources with multiple X-ray observations, although X-ray absorption never vanishes. For a subsample of 11 sources observed at least five times the typical variation time, as defined by a structure function, is less than one year for both heavily absorbed ( $N_H \sim 10^{23} \text{ cm}^{-2}$ ) and moderately absorbed ( $N_H \sim 10^{22} \text{ cm}^{-2}$ ) sources. These variations rule out the simplest version of the unified models, based on a homogeneous obscuring torus, and suggest the presence of clumpy circumnuclear material on a scale well below a parsec. We propose a modification of the torus model in which an overabundance of slightly dusty BELR clouds obscures the BELR. The BELR needs, like the torus, to have an axisymmetric structure. This model is closely related to that of Elvis (2000) for type 1 AGN. For lightly obscured AGN ( $N_H \sim 10^{22} \text{ cm}^{-2}$ ) the structure function shows an increase at a timescale of  $\sim 5$  yr, indicating a second absorber, most probably on a 5-10 pc scale associated with the host galaxy.

*Subject headings:*

## 1. Introduction

Much observational evidence suggests that strong obscuration absorbs the strong continuum source in Active Galactic Nuclei over a significant fraction of the solid angle (Lawrence

---

<sup>1</sup>Harvard-Smithsonian Center for Astrophysics, 60 Garden Street, Cambridge, MA 02138

<sup>2</sup>Dipartimento di Astronomia, Università di Firenze, L.go E. Fermi, 5, I-50125 Firenze, Italy

<sup>3</sup>Osservatorio Astrofisico di Arcetri, L.go E. Fermi, 5, I-50125 Firenze, Italy

& Elvis 1982, Antonucci & Miller 1985, Maiolino et al. 1998). The effects of this absorption are clearly visible in the X-ray spectra of many AGNs, where a photoelectric cutoff at energies of a keV or so (depending on the column density of the gas) is observed, and in the mid-infrared, where we observe the thermal re-emission of the absorbed UV radiation from the dust associated with the absorbing gas. This circumnuclear material obscures the optical emission of the Broad Line Region, but not that of the more distant Narrow Line Region. As a consequence, objects observed along a line of sight covered by this material appear in the optical as type 2 AGNs.

The simplest geometry for this cold gas surrounding the nucleus, is that of a torus covering  $\sim 80\%$  of the solid angle (Antonucci & Miller 1985, Krolik & Begelman 1989). Axial symmetry in the material in the central  $\sim 100$  pc of nearby AGNs is suggested by the biconical shapes (Pogge 1989) seen well in high resolution HST images (Tadhunter & Tsvetanov 1989, Malkan et al. 1998), and polarization requires a highly non-spherical shape (Antonucci & Miller 1985). One of the unsolved questions about the structure of this putative torus is its typical dimensions. Detailed models of homogeneous circumnuclear tori, both on the 1 pc and 100 pc scale, reproduce the observed infrared SED (Pier & Krolik 1992, Granato & Danese 1994). Hard X-ray observations show that at least 50% of nearby Seyfert 2s are obscured by a column density higher than  $10^{24} \text{ cm}^{-2}$  (Risaliti et al. 1999). In these cases it is unlikely that the typical dimensions of a homogeneous torus exceed a few parsecs, since otherwise the dynamical mass of the obscuring material would be too large (Risaliti et al. 1999).

However, detailed observations both in the X-rays and in the near IR/optical band suggest that the structure of the circumnuclear material is more complex than a simple homogeneous torus. Large variations in the cold obscuring column density have been known in a few objects for many years (Ives et al. 1976, Warwick et al. 1988). A more systematic study by Malizia et al. (1997), shows that variations of several  $10^{21} \text{ cm}^{-2}$  are rather common in both type 1 and type 2 Seyferts (17 out of 23 sources observed at least 3 times shows  $N_H$  variations). Changes in months or less suggest much smaller sizes, whether the observed change is due to motions across the line of sight, or to a varying ionization state. The broad emission line region (BELR) has been suggested as a site for this variable absorption in type 1 AGNs (Ives et al. 1976). Since the BELR is either hidden or not present in type 2 AGN this explanation appears implausible for type 2 objects, which comprise 80% of all AGN (Maiolino & Rieke 1995). In this paper we investigate the variability of the X-ray absorbing column density in X-ray-defined Seyfert 2s having column densities higher than  $\sim 10^{22} \text{ cm}^{-2}$ , but less than  $10^{24} \text{ cm}^{-2}$ , i.e. Compton thin. This includes optically defined both types 1.8 and 1.9 objects (which show broad lines only in long wavelength lines, e.g.  $\text{H}\alpha$ ,  $\text{Pa}\alpha$ , Osterbrock 1989) as well as type 2 Seyferts, and all show evidence for cool absorbing

material.

We collected all the data available in the literature for Seyfert 2s and we complemented them with the analysis of unpublished data in the ASCA and BeppoSAX public archives. We found that a sample of 25 sources were observed at least twice in the hard X-rays. 11 objects out of these 25 have 5 or more hard X-ray observations in a time interval of several years, and we can therefore obtain for them an “ $N_H$  light curve”.

In the next Section we show that variations in  $N_H$  are almost universally present. We analyze in greater detail the well-observed 11 sources, dividing them in two subsamples with  $N_H \sim 10^{23} \text{ cm}^{-2}$  (6 objects) and  $N_H \sim 10^{22} \text{ cm}^{-2}$  (5 objects). Previous X-ray studies show that sources with  $10^{22} \text{ cm}^{-2} < N_H < 10^{23} \text{ cm}^{-2}$  are mostly type 1.8 and 1.9 (Risaliti et al. 1999) while those with  $N_H > 10^{23} \text{ cm}^{-2}$  are mostly pure Seyfert 2s. This dichotomy is also present in our sources: 3 out of 5 objects in the low- $N_H$  subsample are intermediate type, while 5 out of 6 in the high- $N_H$  subsample are type 2s (Table 1).

In Section three we analyze the  $N_H$  variability of the well studied subsample using a “Structure Function” similar to that used in studies of brightness variability of quasars (Fiore et al. 1998, Di Clemente et al. 1996). In Section four we discuss our results and we compare them with current models of the circumnuclear medium of AGNs. Our conclusions are summarized in Section 5.

## 2. Data

In Table 1 we list all 139 measurements of  $N_H$  (and 2-10 keV flux) in the literature (with references) for all the 25 Seyfert 2s with  $N_H > 10^{22} \text{ cm}^{-2}$  that have been observed at least twice. Quite a fraction (17 %) of the observations have not previously been published, and their inclusion strengthens our results significantly. Where BeppoSAX or ASCA measurements are not published, we measured the  $N_H$  values through a standard analysis of the data from the BeppoSAX SDC public archive and the ASCA public archive at HEASARC. More details of this analysis will be given in Risaliti (2001, in preparation, see also Appendix A).

For this and subsequent analysis, we used the relevant data from every past X-ray mission. We note that this should not give problems of intercalibration, since the column density is evaluated from the energy of the steep photoelectric cutoff in an X-ray spectrum. Indeed, while the flux calibration between X-ray instruments is notoriously uncertain, the calibration in energy is quite good, especially at energies higher than 1-2 keV, where the instrumental responses do not vary rapidly, and where cut-offs for the  $N_H$  range of these

Seyfert 2s are found.

Figure 1 shows the factor  $f$  by which the column density changes in the sample objects.  $f$  is defined as the ratio between the measured variation of  $N_H$  and the mean of the two values. When more than two observations are available, we chose according to both the size of the variation and the statistical significance: if at least two measurements were different at a confidence level higher than 90%, we chose those with the largest factor variation. Otherwise, we selected the measurements with the most statistically significant variation.

The main result of our analysis is clear from Fig. 1: a significant column density variation on a timescale of years is not a peculiar property of a few sources, but is virtually ubiquitous in Seyfert 2s: only 3 of the 25 Seyfert 2s are consistent with no variation. These have only 2 or 3 observations in the hard X-rays so that variations typical of well-observed sources could easily be missed.

In Figure 2 we plot the relative  $N_H$  and relative 2-10 intrinsic keV flux for each observation of the well observed subsample. Both the measurements are normalized to the average values for each source. The intrinsic flux has been obtained using the best fit values for each observation, and assuming no absorption. Interestingly, no correlation between variations of  $N_H$  and flux appear. If photoionization plays an important role in  $N_H$  variations, we would expect that  $N_H$  values below the average (values  $< 1$  in Fig. 4) are associated to flux measurements above the average (values  $> 1$ ), and vice versa. Therefore, the regions with  $f_x > 1$ ,  $f_y < 1$  and  $f_x < 1$ ,  $f_y > 1$  (top-right and bottom-left quadrants) should be more populated than the regions  $f_x > 1$ ,  $f_y > 1$  and  $f_x < 1$ ,  $f_y < 1$  (top-left and bottom-right quadrants). Instead, the density of points in the four regions is about the same, as expected if flux and  $N_H$  variations are uncorrelated. Moreover, if photoionization effects were important for an object, we would expect a correlation among the points relative to this object. Instead, all the 11 groups of points in Fig. 4 (each of which is marked with a different symbol) appear to be randomly distributed in the  $N_H$ -flux plane. As a further confirmation, we quantitatively estimated the effects of photoionization assuming two different values of the ionization parameter,  $U=0.1$  and  $U=0.5$ , at the inner edge of the absorber. We assumed that the absorber has a total column density  $N_H = 10^{23} \text{ cm}^{-2}$ , distributed on a region  $\sim 5$  times thicker than the distance of the inner edge from the center. These parameters are quite extreme for a “standard” absorber on the parsec scale. They are reasonable if we assume that the absorber is located in the Broad Emission Line Region (BELR). We believe this is a likely possibility, as we show in the following sections. In any case, this scenario can be regarded as extreme in the sense that within it photoionization plays a more important role than in standard torus models. The result we obtained is that fitting the photoionized gas with a cold absorption model, the equivalent cold  $N_H$  changes only of  $\sim 5\%$  if the ioniza-

tion parameter changes from  $U=0.1$  to  $U=0.5$  (a strong continuum variation). Therefore, we conclude that even strong variations in the continuum are not able to cause apparent variations of cold  $N_H$  higher than a few  $10^{21} \text{ cm}^{-2}$ . This further rules out photoionization as a cause of the observed absorption variations.

In order to analyze in greater detail the timescale and the nature of the observed  $N_H$  variations, we focused on a subsample of 11 bright Seyfert 2s with multiple observations in the hard (2-10 keV) X-ray band. Conveniently these 11 sources are divided into two groups: 5 (marked ‘A’ in Table 1) have  $N_H \sim 10^{22} \text{ cm}^{-2}$ , while the other 6 (marked ‘B’) have  $N_H \sim 10^{23} \text{ cm}^{-2}$ . This division is in rough agreement with the optical classification of type 1.8/1.9 for low- $N_H$  objects and type 2s for high- $N_H$  objects (Table 1, Risaliti et al. 1999)

The “light curves” of  $N_H$  are shown for samples A and B in Figures 3 and 4, respectively. The increasing or decreasing of  $N_H$  is not correlated with the instruments used for the measurements, reinforcing the conclusion that the effect is not due to problems in instrumental calibration. Figures 3 and 4 seem to show variations on a variety of timescales from months to years. In Table 2 we list the fastest change in  $N_H$  for each object in the full sample, detected at 90% significance or greater. The objects are sorted according to the observed variation timescale. We note that the shortest variation times are observed in the most extensively studied objects: only 3 out of the 11 sources with 5 or more X-ray observations show variations only on timescales of several years. Therefore, the observed  $N_H$  variability timescales in many objects are only a conservative upper limit: the fastest variations are not detected only because the time delays between the existing observations are too long.

### 3. Structure Function

The data for the two well observed subsamples can be used to obtain a “column density structure function”, defined by analogy with the intensity structure function used to study optical and X-ray variability of QSOs (Di Clemente et al. 1996, Fiore et al. 1998). We considered 10 time intervals,  $t_k$ , for the low  $N_H$  subsample “A” and 11 for the high  $N_H$  subsample “B”, from 1 to 20 years. We defined a *structure function*,  $F(t_k)$ , as the average ratio of all the  $N_H$  measurements separated by a time between  $t_k$  and  $t_{k+1}$  for each set of 5 sources:

$$F(t_k) = \frac{1}{N_k} \sum_{(i,j)} \sum_{l(t_k)} \frac{\max(N_H(j), N_H(l))}{\min(N_H(j), N_H(l))} \quad (1)$$

where  $i$  goes from 1 to 5 in subsample A and from 1 to 6 in subsample B, and labels the source;  $j$  labels the  $N_H$  measurements for each source, while the sum over  $l$  is extended to data  $N_H(l)$  for which the time delay from  $N_H(j)$  is between  $t_k$  and  $t_{k+1}$ .  $N_k$  is the total number of pairs of measurements separated by a time between  $t_k$  and  $t_{k+1}$ . The width of the time intervals was chosen in order to have at least 15 data points per bin.

Since the ratio in the above equation is always greater than 1, the value is biased positive. Following Di Clemente et al. (1996) we remove this bias by defining a modified structure function as follows:

$$F'(t_k) = \sqrt{F(t_k)^2 - \frac{2}{\pi} \langle \sigma_{k,l} \rangle^2} \quad (2)$$

where  $\langle \sigma_{k,l} \rangle$  is the average of the statistical errors on the ratios in Eq. 1.

The Function  $F'(t_k)$  is plotted in Fig. 5a for the low- $N_H$  subsample (A) and in Fig. 5b for the high- $N_H$  sample (B). We removed the points of signal-to-noise less than  $3\sigma$  to avoid an unphysical decrease of  $F'(t_k)$  due to noise. We also used only one of the high 5 signal-to-noise points provided by BeppoSAX observations of the bright source Centaurus A. These observations show a low  $N_H$  variation (although significant at a level higher than 90%), but lower than that measured in average in the other observations. Including all the 5 observations would bias our results since the statistics would be dominated by the single source Centaurus A.

From Fig. 5a and 5b and Fig. 2 we can draw the following conclusions:

1. The variability is statistically highly significant for both the low- $N_H$  and the high- $N_H$  objects at all the timescales considered (90 days - 20 years).
2. For both samples the variability is already significant at the shortest timescale that can be investigated with our data (several months). This result is also confirmed by the data in Table 2 for to the whole sample: sources with measured variations in a time shorter than 1 year are  $\sim 50\%$  of the whole sample, rising to  $\sim 70\%$  of the subsample of sources for which we actually have observations within a time interval of less than 1 year.
3. The modified structure function is constant (within statistical errors) for the high  $N_H$  sample, while for the low  $N_H$  sources it seems to have a significant increase for  $t_k > 5$  years. This suggests a characteristic timescale of  $\sim 5$  years for variations in the order of  $10^{22} \text{ cm}^{-2}$ , since the structure function is expected to increase with time when a slower variation is convolved (randomly) with faster ones.

4. Despite the large  $N_H$  variability observed, no object has been observed to change from type 1 to type 2 (i.e.  $N_H$  never drops below several  $10^{21} \text{ cm}^{-2}$ )
5. Variations of  $N_H$  are not correlated with X-ray flux variations (Fig. 2).

## 4. Discussion

### 4.1. The distance from the center of the obscuring gas

In the previous Section we demonstrated that  $N_H$  variability in a timescale from months to years is present in the great majority, and possibly in all, Seyfert 2 galaxies. The structure function described in the previous section is useful to quantify the general  $N_H$  variability properties of our sources. A physical interpretation of our results must explain both the shape of this function and the different properties of the individual sources.

There are two physical reasons that can explain the variability of the absorbing column density: variations in the ionization state of the absorber, due to variations in the ionizing radiation, and variations in the amount of absorbing gas along the line of sight. In the first case, the absorber can be homogeneous, and the variation in  $N_H$  should be correlated with intrinsic flux variations. In the second case, the absorber must be clumpy, and the variation timescales will be correlated with the typical crossing time of an absorbing cloud along the line of sight. However we already showed that a change in ionization does not fit the data (Section 2, Fig. 2) We can therefore adopt the second scenario -motions in a clumpy medium- and use the information collected in the previous sections to estimate the distance from the center of the obscuring gas.

We can idealize the situation by assuming the typical timescale of variation,  $t$ , to be the crossing time of a discrete cloud across the line of sight. Assuming that the absorption is due to spherical clouds moving with Keplerian velocities, the distance from the central black hole of mass  $M$  is given by:

$$R \sim 3 \times 10^{16} \frac{M_{\bullet}}{10^9 M_{\odot}} \left( \frac{\rho}{10^6 \text{ cm}^{-3}} \right)^2 \left( \frac{t}{5 \text{ Msec}} \right)^2 \left( \frac{N_H}{10^{22} \text{ cm}^{-2}} \right)^{-2} \text{ cm} \quad (3)$$

where  $\rho$  is the density of the cloud. The black hole mass and the cloud density have been normalized to extreme values for a putative torus (Krolik & Begelman 1989) in order to obtain the greatest distance. The black hole mass  $M_{\bullet} = 10^9 M_{\odot}$  is obtained from mass measurements of central black holes in nearby galaxies (Kormendy & Richstone 1998). The typical average density  $\langle \rho \rangle$  in a standard torus can be evaluated as the ratio between the column density and the thickness of the torus. Objects of subsample B have  $N_H \sim$  several

$10^{23} \text{ cm}^{-2}$ , then  $\rho_{AV} \sim 10^5 \text{ cm}^{-3}$ . Given the clumpiness of the torus, the actual density of a cloud can be higher, however the value  $\rho = 10^6 \text{ cm}^{-3}$  can be regarded as an upper limit. Even though most of the physical parameters in the equation above are poorly constrained, several conclusions can nevertheless be drawn. First, the shorter timescale  $N_H$  variations ( $\sim 2$  month or less) must be due to material that is nearer to the center than about  $10^{17} \text{ cm}$ , while the radius of the standard model torus is 1-3 pc (Krolik & Begelman 1992). The only physical parameter that can reasonably be larger, assuming different physical conditions, is the cloud density: for example, photoionization models suggest that BELR clouds have  $\rho \geq 10^9 \text{ cm}^{-3}$  (Netzer 1990). Even in this case though it is hard to imagine a reasonable geometry with distances larger than  $\sim 10^{17} \text{ cm}$ , since this would imply that the absorbing material is confined in a thin slab whose depth is less than  $10^{-4}$  of the distance from the center, but covering a large solid angle.

These parameters are even better constrained for two of the objects in our sample for which a measurement of the black hole mass is available: Centaurus A ( $M_{\bullet} = 2_{-1.4}^{+3} 10^8 M_{\odot}$ , Marconi et al. 2001) and NGC 4258 ( $M_{\bullet} = 4.2 \pm 0.2 10^7 M_{\odot}$ , Miyoshi et al. 1995). Using the fastest  $N_H$  variations observed (which are only upper limits to the actual variation timescales) we obtain:

$$R_{\text{CENA}} \leq 2 \times 10^{15} \left( \frac{\rho}{10^6 \text{ cm}^{-3}} \right)^2 \text{ cm} \quad (4)$$

and

$$R_{\text{N4258}} \leq 7 \times 10^{16} \left( \frac{\rho}{10^6 \text{ cm}^{-3}} \right)^2 \text{ cm} \quad (5)$$

These results pose severe problems to the standard torus model, according to which the X-ray absorption is due to cold gas distributed in a toroidal geometry on the parsec scale.

An alternative possibility, within the standard AGN model (Antonucci 1993) is that the X-ray absorber is located in the broad emission line region, much nearer to the central black hole than the “standard” torus. An indication for an absorber on the BELR scale is also provided by recent high resolution soft X-ray spectra obtained with XMM-Newton (Sako et al. 2001). If we assume that the broad line clouds are responsible for the absorption in the X-rays, we can find a consistent combination of the parameters in Eq. 1. For example, assuming  $\Delta N_H \sim 10^{23} \text{ cm}^{-2}$ ,  $M=10^7 M_{\odot}$ ,  $\rho = 10^9 \text{ cm}^{-3}$ , typical for Seyfert galaxies (Netzer 1990), and  $t=5$  days we obtain  $R \sim 3 \times 10^{16} \text{ cm}$ ,  $\sim 3$  light days, a distance typical for the BELR based on reverberation mapping (Peterson et al. 1997). Our point can be graphically illustrated as in Fig. 6, where we show that our observed variability is not compatible with a parsec-scale torus, while a variability of  $\sim 1$  day could be in agreement with an absorber located in the BELR.

The typical column density of the obscuring clouds also lies in the regime of BELR



clouds. This variability consequently requires that the circumnuclear absorber is not homogeneous, but clumped into several clouds. Assuming Gaussian fluctuations, the average number of clouds along the line of sight,  $N_C$ , should be of the order  $(1/f)^2$ . The right hand axis of Fig. 1 shows this number to be of order a few for most of the sample. In no case though, even for  $N_C < 1$ , did  $N_H$  drop below  $5 \times 10^{21} \text{ cm}^{-2}$ , well above the lowest detectable value for these observations. Therefore, despite the large variability in  $N_H$ , there are no changes from type 2 to type 1. From Fig. 1 we estimate that the average column density of the single clouds,  $N_{HC} = \langle N_H \rangle / N_C$ , range from a few  $10^{21} \text{ cm}^{-2}$  in low- $N_H$  objects, up to several  $10^{23} \text{ cm}^{-2}$  in high  $N_H$  objects. We report the estimates of  $N_{HC}$  in the last column of Table 2. The  $N_{HC}$  distribution is plotted the histogram in Fig. 7.

However, the standard model for AGNs fails to explain X-ray absorption through the broad line clouds because it would predict several unseen features. Photoionization models require that in type 1 AGNs the covering factor of the broad line clouds (assuming an isotropic distribution around the central black hole) is typically 10% and certainly much lower than 100%. We would then expect that (1) 10% of type 1 AGNs would be X-ray absorbed, and (2), repeated observations of the same object would reveal, in 10% of the cases, an X-ray absorbed spectrum. At present about 20 bright Seyfert 1s have been extensively studied in the X-rays for several years, by means of several X-ray observatories (Turner & Pounds 1989, Nandra & Pounds 1989, Nandra et al. 1997), and these effects have been observed only in one case (NGC 3516, Costantini et al. 2000). In the optical, where many more objects have been extensively observed, there are only few known cases of transition from type 1 to type 2 or vice versa (NGC 7603, Tohline & Osterbrock 1976; MKN 1018, Cohen et al. 1986; NGC 7582, Aretxaga et al. 1999; for other cases see references in Aretxaga et al. 1999). We conclude that the standard AGN model is not able to reproduce the observed variability of X-ray absorption in Seyfert 2 galaxies.

## 4.2. Alternative scenarios

From the discussion above we conclude that the observed X-ray variability must be explained by an absorber with the following properties: (1) close to the central engine (unless moving faster than Keplerian), (2) clumped (to explain the  $N_H$  variability, with  $N_C \sim 10$ ), (3) covers a significant fraction,  $\sim 0.8$ , of the solid angle (in order to reproduce the 4:1 ratio between Seyfert 2s and Seyfert 1s), and (4) since AGN rarely change from type 2 to type 1, the absorber cannot be spherically symmetric so that the 80% of lines of sight covered must always remain the same.

#### 4.2.1. Type 2 AGNs from an excess of broad line clouds

A straightforward extension of the standard unified model that can reproduce the right X-ray absorption properties is to suppose that in Seyfert 2s the BELCs are, somewhat paradoxically, *much more numerous* than in Seyfert 1s, so that the covering factor is 100% and on average several clouds cover the line of sight.

We can repeat the argument used above to rule out the parsec-scale torus, to constrain the variability timescales within this model: assuming that the absorber is made by BELCs ( $\rho \sim 10^9 \text{ cm}^{-3}$ ) moving with Keplerian velocity, we can obtain a consistent distance from the center only assuming variations on timescales of days. Assuming a typical velocity of  $5000 \text{ km s}^{-1}$  for the BELCs, the crossing time of a cloud is  $t \sim 6(\frac{\rho}{10^9 \text{ cm}^{-3}})^{-1}(\frac{N_H}{10^{22} \text{ cm}^{-2}})$  days, and the distance from the center is  $R \sim 5 \times 10^{16} \frac{M_\bullet}{10^8 M_\odot} \text{ cm}$ .

Rewriting Equation 3 for a BELR absorber, and using a typical  $N_H$  variation for the high- $N_H$  subsample, we have:

$$R \sim 4 \times 10^{16} \frac{M_\bullet}{10^8 M_\odot} \left(\frac{\rho}{10^9 \text{ cm}^{-3}}\right)^2 \left(\frac{t}{1 \text{ day}}\right)^2 \left(\frac{N_H}{5 \times 10^{22} \text{ cm}^{-2}}\right)^{-2} \text{ cm} \quad (6)$$

Such a model is novel because would ascribe the differences between type 1 and type 2 AGNs to physical properties, rather than to orientation effects. Orientation is reintroduced because the X-ray absorber cannot be spherically distributed around the center (because of the shortage of objects changing from type 1 to type 2 and vice versa, as outlined in the previous Section).

The simplest possible geometry for a non-spherically symmetric absorber is axisymmetric: a bi-cylinder or a bi-cone. This geometry is appealing because the same structure has been recently proposed by Elvis (2000) in order to explain the absorption and scattering properties of type 1 AGNs. According to this model, some disk instability generates a two-phase wind from a narrow range of disk radii: the warm phase, with temperatures of the order of  $\sim 10^5 - 10^6 \text{ K}$ , is responsible for most of the scattering phenomena observed in AGNs, and for both the UV narrow absorption lines and the X-ray warm absorbers seen in a significant fraction of type 1 AGNs by the Hubble Space telescope (Crenshaw et al. 1999) and ASCA (Reynolds 1998). The cold phase of the wind is formed by the BELCs (Figure 8). A simple extension of this model could be that in type 2 AGNs the BELCs confined the warm wind are far more common and completely cover all lines of sight, i.e. on average more than one cloud is present along each line of sight. The fraction of matter in the different phases of multi-phase media, e.g. the ISM, is not predictable with current theory, and may be history dependent. Some alteration in the seed medium produced by a change in the disk

instability at least provides a plausible site for such a bi-modal state to originate. A variation of this is that a larger radial thickness of the wind might produce the dichotomy between type 1 and type 2 AGN. In this case, the average distance of the center of the X-ray absorber could be significantly larger than the distance of the BELR, since the BELCs will be only those located close to the inner edge of the wind (Fig. 8). Indeed, indications of a large thickness of the BELR come also from reverberation mapping studies, according to which low ionization lines, as  $\text{MgII } \lambda 2800\text{\AA}$ , are emitted by a region several times farther from the center than that emitting high ionization lines like  $\text{HeII } \lambda 1640\text{\AA}$  and  $\text{NV } \lambda 1240\text{\AA}$  (Peterson 1993).

An interesting prediction of this model is that the change from type 2 to type 1 could occasionally happen, when the line of sight is freed from clouds, because of random motions. In these cases, broad lines in the optical and soft X-rays outburst would be observable. The duration of these breaks in the clouds is of the same order of the crossing time of a cloud along the line of sight. Assuming the parameters used in Eq. 2, and a column density for a single cloud of  $\sim 10^{22} \text{ cm}^{-2}$ , we can estimate this time to be  $t \sim 1$  day, too short to be caught with anything but the most intense monitoring. The probability  $P$  that this happens depends on the average number of clouds  $N_C$  along the line of sight. Assuming  $N_C=4$  and  $N_C=10$  (two plausible values, see Fig. 1) we have  $P \sim 1\%$  and  $P \sim 0.01\%$ , respectively. A detailed study of this case will be presented in Nicastro et al. 2001 (in preparation).

A problem with this “many clouds” model comes from the optical emission of Seyfert 2s. AGNs that are obscured only by the broad line cloud gas should not be obscured in the optical continuum, but only in the resonant lines themselves. But Seyfert 2s continua are weak (Koski 1978). Instead Seyfert 2s clearly suffer extinction due to dust (Peterson 1997). Some dust must then be present in the BELCs of type 2 AGN. Certainly the outer layers of clouds are heavily shielded from the ionizing continuum and could be the locus of dust formation, although the timescales required in our case are probably too short. Another possibility is that the material inflowing from the host galaxy and feeding the AGN is dusty, and part of the dust is transferred to the external part of the wind, that is much thicker and farther from the center than in the “optically thin” model of Elvis 2000. Therefore, part of the dust could survive until it reaches the wind. The amount of inflowing material could be the physical quantity that tunes the thickness of the wind, thus determining the type 1 or type 2 classification. This possibility is interesting, given the growing evidence suggesting a low dust to gas ratio in the absorbing medium of many AGNs (Maiolino et al. 2000, Risaliti et al. 2001). A dust poor absorber, located close to the central black hole, has already been suggested by Granato et al. (1997). These authors show that the infrared emission of Seyfert 2s is best reproduced assuming a low dust-to-gas ratio, and suggest that most of the X-ray absorber is located inside the AGN sublimation radius.

Our “intrinsic” model for the difference between type 1 and type 2 AGN also explains the otherwise puzzling lack of strong infrared dust emission observed in most Seyfert 1s. Edelson et al. (1987) show that only about 1/3 of Seyfert 1s show strong dust contribution to infrared emission in IRAS. This observational fact is hard to include in the standard unified models: Seyfert 1s should have the same obscuring tori as Seyfert 2s, and therefore their infrared emission should be of the same order of that of Seyfert 1s, with respect to the bolometric intensity. The model we proposed predicts that orientation apply only to objects with “many” clouds, that are type 2 if seen through the wind and type 1 (with high IR dust emission) if seen pole-on. Objects with “few” clouds are type 1 along every line of sight, and are not expected to be strong IR emitters. Finally, this scenario is appealing because it predicts a link between the absorbing column density and the amount of material inflowing from the host galaxy, in agreement with the finding that heavily absorbed AGNs are preferentially hosted in strongly barred galaxies (Maiolino et al. 1999).

Within this model we can estimate the fraction  $f$  of objects with “many” clouds and the average opening angle,  $\alpha$ , of the wind (Fig. 8). Using the ratio 4:1 between type 2s and type 1s (Maiolino et al. 1995) and the fraction 1/3 for the dust emitting type 1s (Edelson et al. 1987) we obtain  $\alpha \sim 25^\circ$  and  $f \sim 85\%$ . We note that the opening angle of the wind in the model of Elvis 2000 is higher ( $\sim 60^\circ$ ). However, the presence of a second absorber (see next Section) can reduce this discrepancy.

#### 4.2.2. A second, large scale, absorber

The increase in the  $N_H$  structure function for low  $N_H$  objects at  $t \sim 5$  years is not explained by a “many clouds”, BELR, origin for the cold X-ray absorber. Instead an additional, second, absorber is needed, located much farther from the center. Inhomogeneities in this absorber could be related to the long term variability on timescales of years revealed in our sample of objects with  $N_H \sim 10^{22} \text{ cm}^{-2}$ . Assuming a column density variation of  $5 \times 10^{21} \text{ cm}^{-2}$  (typical for the long-timescale variations observed in the low- $N_H$  subsample), we can parametrize the distance from the center of this second absorber as follows:

$$R \sim 10^{19} \frac{M_\bullet}{10^8 M_\odot} \left( \frac{\rho}{10^6 \text{ cm}^{-3}} \right)^2 \left( \frac{t}{5 \text{ yr}} \right)^2 \left( \frac{N_H}{5 \times 10^{21} \text{ cm}^{-2}} \right)^{-2} \text{ cm} \quad (7)$$

This absorber can be compatible with the standard torus model ( $R \sim 10^{19} \text{ cm}$ ), in objects with a lower  $M_\bullet$  or with a lower cloud density.

The existence of a second absorber is needed by the BELC-origin model, that, in the

original version of Elvis (2000) implies a covering factor of  $\sim 0.5$  and so cannot reproduce the high ratio between Seyfert 2s and Seyfert 1s, which is known to be  $\sim 4$  for nearby objects (Maiolino & Rieke 1995). Moreover, strong suggestions of the existence of two distinct absorbers come from the analysis of the X-ray spectra of several nearby AGNs (Malaguti et al. 1999, Turner et al. 2000, Vignali et al. 1998). The orientations of the two absorbers are likely unrelated, since neither radio jet axes nor emission line bi-cones (Pogge 1989) align with galaxy minor axes (Ulvestad & Wilson 1984). There will then be objects obscured only by one of the two absorbers. This obviously would increase the fraction of obscured lines of sight. Objects obscured only by the more distant medium cannot have column density variations in timescales of days. This is in agreement with the measurements described in the previous sections.

A consequence of this second absorber is that the ratio between free and wind-covered lines of sight can be higher than predicted in the previous Section, since some fraction of the objects are type 2 because they are covered by the farther absorber. This would reduce the opening angle discrepancy between our model and that of Elvis (2000). We can give a quantitative estimate of this effect if we assume that intermediate type objects ( $\sim$  sample A) are those observed through the outer torus, but not through the wind. We therefore have a new, lower, ratio between type 1.8-2 and type 1-1.5 objects, and an estimate of the covering factor of the outer obscurer from the ratio between intermediate and type 1 Seyferts. With these number we calculate an half-opening angle of  $35^\circ$  and a fraction of objects with “many clouds”  $f=75\%$ . The half-opening angle is still significantly lower than in the model by Elvis (2000). However, we note that in the Elvis model the wind is turned by radiation pressure. We expect that the wind in our model, more massive than that of Elvis (2000), is harder to turn by radiation pressure.

## 5. Conclusions

In this paper we have shown that large amplitude (20-100%), rapid ( $\lesssim$  months) variability of X-ray absorbing column density is an almost ubiquitous property of Seyfert 2 galaxies. From our compilation of 25 objects with at least 2 observations in the hard X-rays (2-10 keV) we found that in 21 cases the  $N_H$  varies at a confidence level greater than 90%. We demonstrated that the variations of  $N_H$  are not related to the underlying X-ray flux and so are not due to variations in the ionization state of the absorber. Variations of the amount of absorbing gas along the line of sight is the only obvious alternative. Our result requires the absorbing gas to be clumpy (in order to reproduce the observed variability) and its distribution around the black hole cannot be spherically symmetric (since changes from type 2

to type 1 are not observed in the X-rays).

For a well observed subsample of 11 sources with at least 5 observations in the hard X-rays, the structure function shows that the typical variation timescales are shorter than several months. The data do not probe shorter timescales well, so this is an upper bound. The shortest measured variation is less than 1 year for 70% of the sources for which this can be measured.

From the structure function of the low  $N_H (< 10^{23} \text{ cm}^{-2})$  sample we also find an indication of the presence of a larger scale absorber, responsible for  $N_H$  variations on timescales of the order of  $\sim 5$  years.

The fast variability is incompatible with the standard parsec-scale torus of unified models. In order to reproduce the observed X-ray properties, the absorbers have to be clumpy and close to central black hole (distance  $R < 10^{17} \text{ M}_\bullet/\text{M}_\odot \text{ cm}$ ).

We propose a model in which a superabundance of broad emission line region clouds produces the absorption. The bi-cylindrical geometry of Elvis (2000), in which the absorber is the cold phase of a wind arising from the accretion disk reintroduces orientation as a factor in whether we see a type 1 or a type 2 AGN. The model we proposed also predicts that a change from type 2 to type 1 could occasionally be observable in the X-rays (further details will be in Nicastro et al. 2001, in preparation).

We found significant variability of  $N_H$  on all the timescales that we could investigate. Moreover, the model we propose predicts  $N_H$  variability in timescales of days. Therefore, this work can be usefully complemented by an analysis of the  $N_H$  variations at shorter timescales. Several observations made with ASCA and BeppoSAX have a sufficient statistics to look for  $N_H$  variations of timescales from  $\sim 10,000$  seconds to 2 days. A more detailed study on this issue will be the subject of a forthcoming paper (Risaliti et al. 2001, in preparation).

This work has made use of data obtained through the Science Data Center of the Italian Space Agency and the High Energy Astrophysics Science Archive Center (HEASARC) online archive, provided by NASA-Goddard Space Flight Center. This work was supported in part by NASA grant NAG5-4808. aastex-help@aas.org.

## A. New hard X-ray measurements

22 measurements listed in Table 1 (4 with ASCA and 18 with BeppoSAX) are previously unpublished. These data permit the inclusion in the sample of two heavily obscured objects

(NGC 4941 and NGC 3081) and are also important for the statistical significance of the structure function, since almost all the spectra have an high signal to noise, allowing  $n_H$  measurements among the most precise in all sample.

The data analysis was performed using a standard technique:

- *ASCA data*: we only analyzed the two GIS (0.7-10 keV) observations, extracting a spectrum from a circular region of radius 4' centered on the source. The background was obtained from a free region in the same field. The data were rebinned in order to have at least 20 counts per channel.

- *BeppoSAX data*: we analyzed the data from the LECS (0.1-10 keV) , MECS (1.65-10.5 keV) and PDS (20-200 keV) instruments. We extracted a spectrum from the LECS and MECS data using a region equal to that used for the ASCA data. We used the PDS spectrum provided by the SAX Science Data Center (SDC).

- *Models*: we fitted the data with a baseline model composed by an absorbed power law plus a thermal component. In many cases, given the high signal to noise of the spectra, several featured are clearly non fitted. In order to obtain a good fit, we added extra components to the baseline model (a Gaussian emission line to fit the iron  $K\alpha$  emission at  $E \sim 6.4$  keV, a cold reflection component, an high energy cutoff for sources observed with BeppoSAX). We give a detailed description of these fits in another paper (Risaliti 2001, in preparation). The important point for the measures used in this work is that in all cases we finally obtained a statistically acceptable fit, and the  $N_H$  measurements are not significantly affected by the details of the fit of the other spectral components.

## REFERENCES

- Akylas, A., Georgantopoulos I., & Comastri A. 2000, MNRAS, 324, 521
- Aretxaga, I., Joguet, B., Kunth, D., Melnick, J., & Terlevich, R.J. 1999, ApJ, 519, 123
- Antonucci, R.R.J., & Miller, J. 1985, ApJ, 297, 621
- Antonucci, R.R.J. 1993, ARA&A, 31, 473
- Awaki, H., Koyama, K. 1993, Adv. Space Res, 13, 221
- Awaki, H., Ueno, S., Taniguchi, Y., Weaver, K.A. 2000, ApJ, 542, 175
- Baity, W.A., et al. 1981, ApJ, 244, 429

- Bassani, L., Dadina, M., Maiolino, R., Salvati, M., Risaliti, G., Della Ceca, R., Matt, G., Zamorani, G. 1999, *ApJS*, 121, 473
- Cohen, R.D., Puetter, R.C., Rudy, R.J., Ake, T.B., & Foltz, C.B. 1986, *ApJ*, 311, 135
- Costantini, E., et al. 2000, *ApJ*, 544, 283
- Crenshaw, D.M., Kraemer, S.B., Boggess, A., Maran, S.P., Mushotzky, R.F., & Wu, C.C. 1999, *ApJ*, 516, 750
- Lawrence, A., & Elvis, M. 1982, *ApJ*, 256, 410
- Di Clemente, A., Giallongo, E., Natali, G., Trevese, D., & Vagnetti, F. 1996, *ApJ*, 463, 466
- Edelson, R.A., Malkan, M.A., & Rieke, G.H. 1987, *ApJ*, 321, 233
- Elvis, M. 2000, *ApJ*, 545, 63
- Fiore, F., Laor, A., Elvis, M., Nicastro, F., & Giallongo, E. 1998, *ApJ*, 503, 607
- Forster, K., Leighly, K.M., & Kay, L.E. 1999, *ApJ*, 523, 521
- Georgantopoulos, I., & Papadakis, I.E. 2000, *MNRAS*, 322, 218
- Gilli, R., Maiolino, R., Marconi, A., Risaliti, G., Dadina, M., Weaver, K.A., & Colbert, E.J.M. 2000, *A&A* 355, 485
- Granato, G.L., Danese, L. 1994, *MNRAS*, 268, 235
- Granato, G.L., Danese, L., & Franceschini, A. 1997, *ApJ*, 486, 147
- Halpern, J.P. 1981, Ph.D Thesis, Harvard University
- Ives, J.C., Sanford, P.W., & Penston, M.V. 1976, *ApJ*, 207, L159
- Iwasawa, K., Fabian, A.C., Mushotzky, R.F., Brandt, W.N., Awaki, H., & Kunieda, H. 1996, *MNRAS*, 279, 837
- Iyomoto, N., Makishima, K., & Fukazawa, Y. 1997, *PASJ*, 48, 425
- Krolik, J.H. 1999, “Active galactic nuclei : from the central black hole to the galactic environment”, Princeton University Press
- Krolik, J.H., & Begelman, M.C. 1988, *ApJ*, 329, 702



- Malizia, A., Bassani, L., Stephen, J.B., Malaguti, G., & Palumbo, G.G.C. 1997, *ApJ*, 113, 311
- Maiolino, R., & Rieke, G.H. 1995, *ApJ*, 454, 95
- Maiolino, R., Salvati, M., Bassani, L., Dadina, M., Della Ceca, R., Matt, G., Risaliti, G., & Zamorani, G. 1998, *A&A*, 338, 781
- Maiolino, R., Risaliti, G., & salvati, M. 1999, *A&A*, 241, L35
- Maiolino, R., Marconi, A., Salvati, M., Risaliti, G., Severgnini, P., Oliva, E., La Franca, F., Vanzi, L. 2001, *A&A*, 365, 28
- Malaguti, G., Bassani, L., & Caroli, E. 1994, *ApJS*, 94, 517
- Malaguti, G., et al. 1999, *A&A*, 344, 857
- Malkan, M.A., Gorjian, M., & Tam, R. 1998, *ApJS*, 117, 25
- Marconi, A., Capetti, A., Axon, D., Koekemoer, A., Macchetto, F.D., & Schreier, E.J. 2001, *ApJ*, 549, 915
- Miyoshi, M., Moran, J., Herrnstein, J., Greenhill, L., Nakai, N., Diamond, P., & Inoue, M. 1995, *Nature*, 373, 127
- Morini, A., F., & Molteni, D. 1989, *ApJ*, 347, 750
- Mulchaey, J.S., Colbert, E., Wilson, A.S., Mushotzky, R.F., & Weaver, K.A. 1993, *ApJ*, 414, 144
- Mushotzky, R.F., Serlemitsos, P.J., Becker, R.H., Boldt, E.A., & Holt, S.S. 1978, *ApJ*, 220, 790
- Nandra, K., George, I.M., Mushotsky, R.F., Turner, T.J., & Yaqoob, T. 1997, *ApJ*, 476, 70
- Peterson, B.M. 1993, *PASP*, 105, 247
- Peterson, B.M. 1997, “An introduction to active galactic nuclei”, Cambridge University Press.
- Pier, E.A., & Krolik, J.H. 1992, *ApJ*, 401, 99
- Pogge, R.W. 1989, *ApJ*, 345, 730
- Reynolds, C.S. 1997, *MNRAS*, 286, 513

- Reynolds, C.S., Nowak, M.A., & Maloney, P.R. 1998, *ApJ*, 540, 143
- Risaliti, G., Maiolino, R., & Salvati, M. 1999, *ApJ*, 522, 157
- Risaliti, G., Maiolino, R., & Bassani, L. 2000, *A&A*, 356, 33
- Risaliti, G., Marconi, A., Maiolino, R., Salvati, M., & Severgnini, P. 2001, *A&A*, 371, 37
- Sambruna, R.M., Eracleous, M., & Mushotzky, R.F. 1999, *ApJ*, 526, 60
- Severgnini P., Risaliti G., Marconi A., Maiolino R., & Salvati M. 2000, *A&A*, 368, 44
- Singh, K.P., Garmire, G.P., & Nousek, J. 1985, *ApJ*, 297, 633
- Smith, D.A., & Done, C. 1996, *MNRAS*, 280, 355
- Stark, J.P.W., *Proc. R. Soc. Lond. A.*, 366, 435
- Tadhunter, C., & Tsvetanov, Z. 1989, *Nature*, 341, 422
- Tohline, J.E., & Osterbrock, D.E. 1976, *ApJL*, 210, L17
- Turner, T.J., & Pounds, K.A. 1989, *MNRAS*, 240, 833
- Turner, T.J., George, I.M., Nandra, K., & Mushotsky, R.F. 1997, *ApJS*, 113, 23
- Turner, T.J., Perola, G.C., Fiore, F., Matt, G., George, I.M., Piro, L., & Bassani, L. 2000, *ApJ*, 531, 245
- Ulvestad, J.S., & Wilson, A.S. 1984, *ApJ*, 277, 92
- Vignali, C., Comastri, A., Stirpe, G.M., Cappi, M., Palumbo, G.G.C., Matsuoka, M., Malaguti, G., & Bassani, L. 1998, *A&A*, 331, 411
- Warwick, R.S., Pounds, K.A., & Turner, T.J. 1988, *MNRAS*, 231, 1145
- Warwick, R.S., Pounds, K.A., Sembay, S., Yaqoob, T., Makishima, K., Ohashi, T., Tashiro, M., & Komhura, Y. 1993, *MNRAS*, 265, 412
- Weaver, K.A.: Ph.D Thesis, University of Maryland
- Weaver, K.A., Arnaud, K.A., & Mushotsky, R.F. 1995, *ApJ*, 447, 121
- Wilkes, B.J., Mathur, S., Fiore, F., Antonelli, A., & Nicastro, F. 2000, *ApJ*, 549, 248
- Xue, S., Otani, C., Mihara, T., Cappi, M., & Matsuoka, M. 1998, *PASJ*, 50, 519



Fig. 1.— Ratio between the variation of  $N_H$  and the mean  $N_H$  for all the Seyfert 2s with multiple hard X-ray observations. Empty circles are used for sources with only 2 or 3 observations in the hard X rays, full circles for sources with 4 or more observations.

On the right y-axis we report the expected average number of clouds along the line of sight, assuming Poissonian fluctuations.

Fig. 2.—  $N_H$  light curves for a subsample of 5 Seyfert 2s with  $N_H \sim 10^{22} \text{ cm}^{-2}$  and multiple hard X-ray observations.

Fig. 3.—  $N_H$  light curves for a subsample of 5 Seyfert 2s with  $N_H \sim 10^{23} \text{ cm}^{-2}$  and multiple hard X-ray observations.

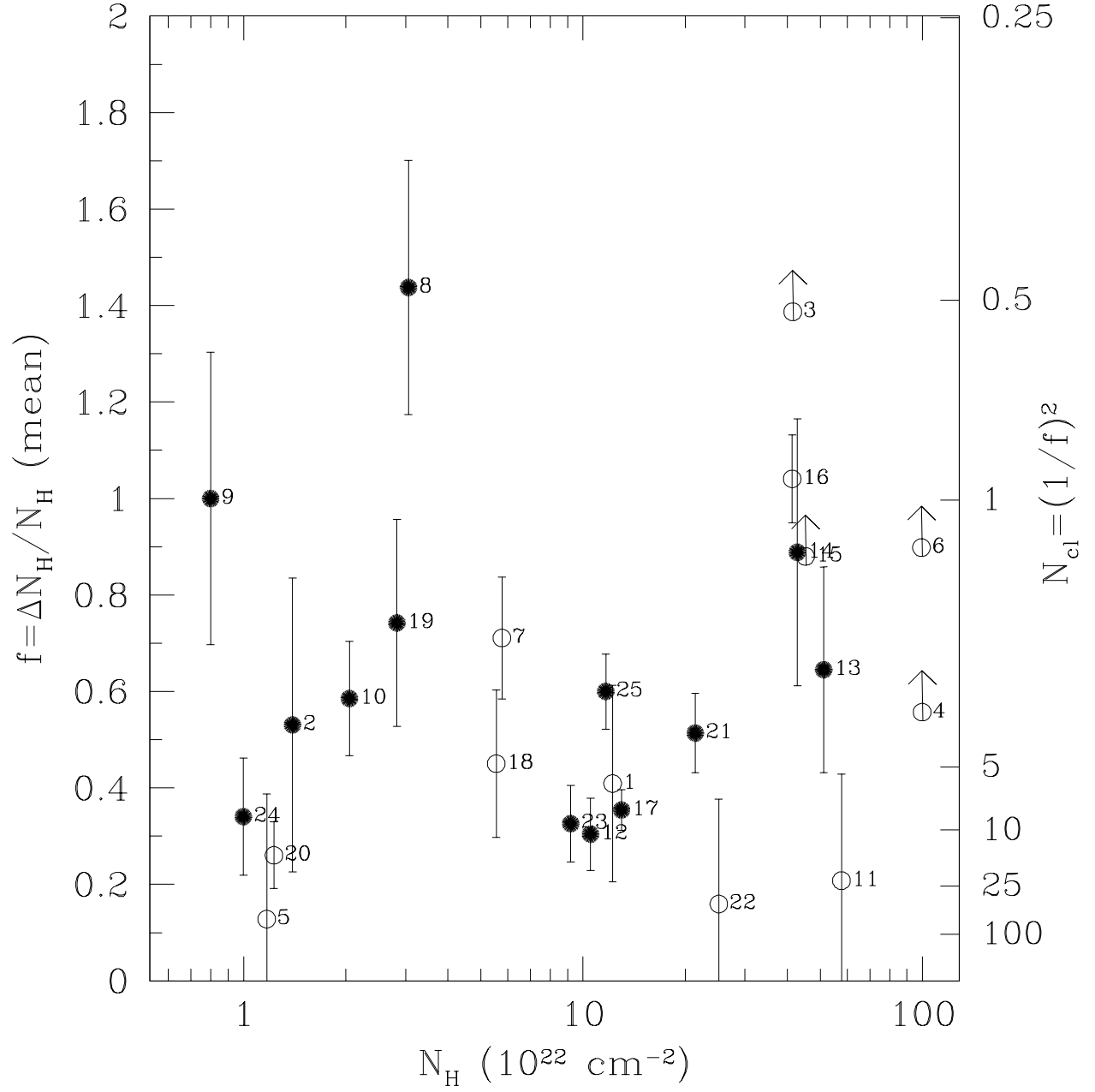
Fig. 4.—  $N_H$  versus 2-10 keV flux for the observations of the well observed subsample. Both  $N_H$  and flux are normalized to the average value for each source. Different symbols are used for each of the 11 sources of the subsample.

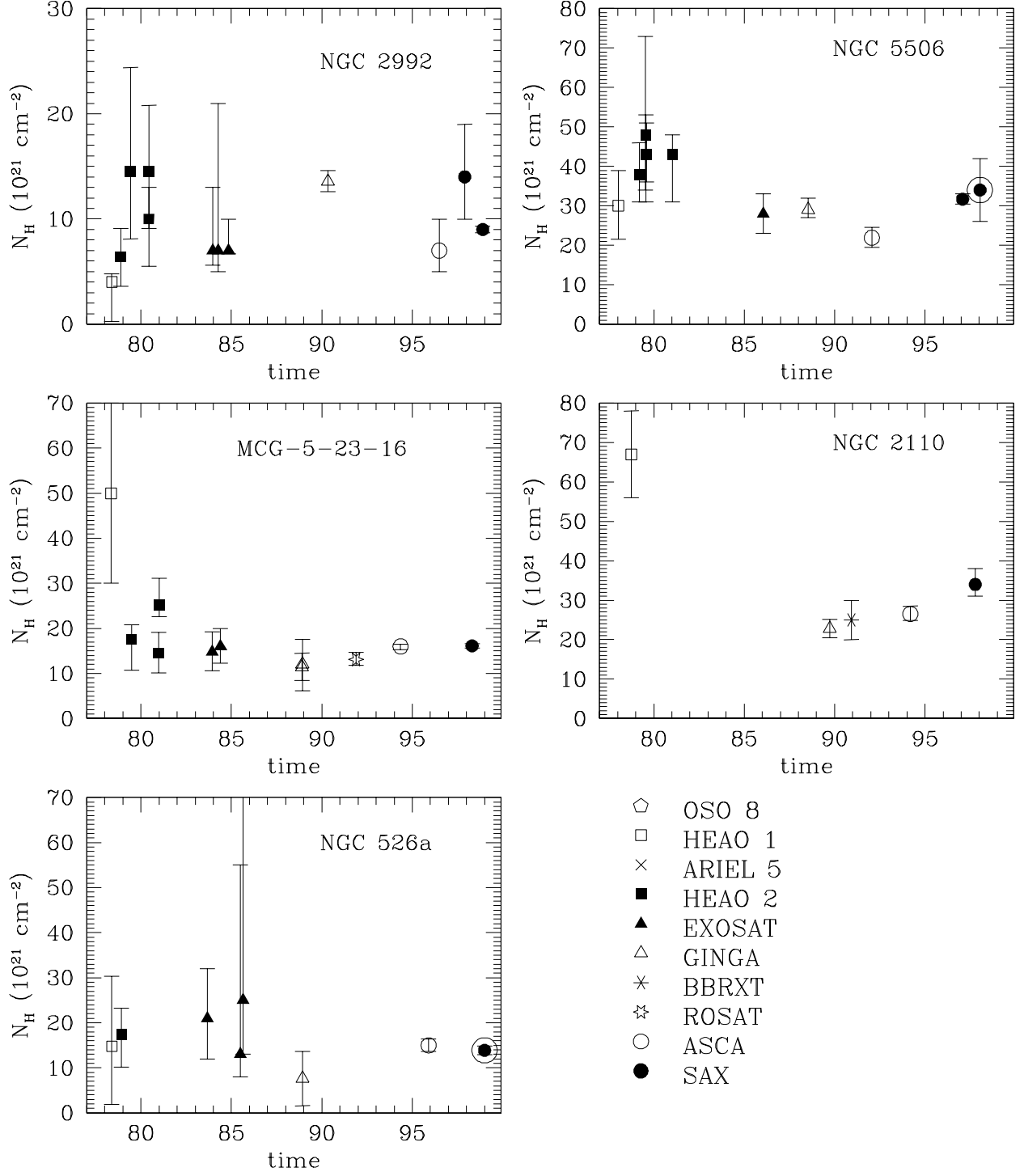
Fig. 5.— Structure function for the Column density variations (see text for definitions). Panel (A): subsample with  $N_H \sim 10^{22} \text{ cm}^{-2}$ . Panel (B): subsample with  $N_H \sim 10^{23} \text{ cm}^{-2}$ .

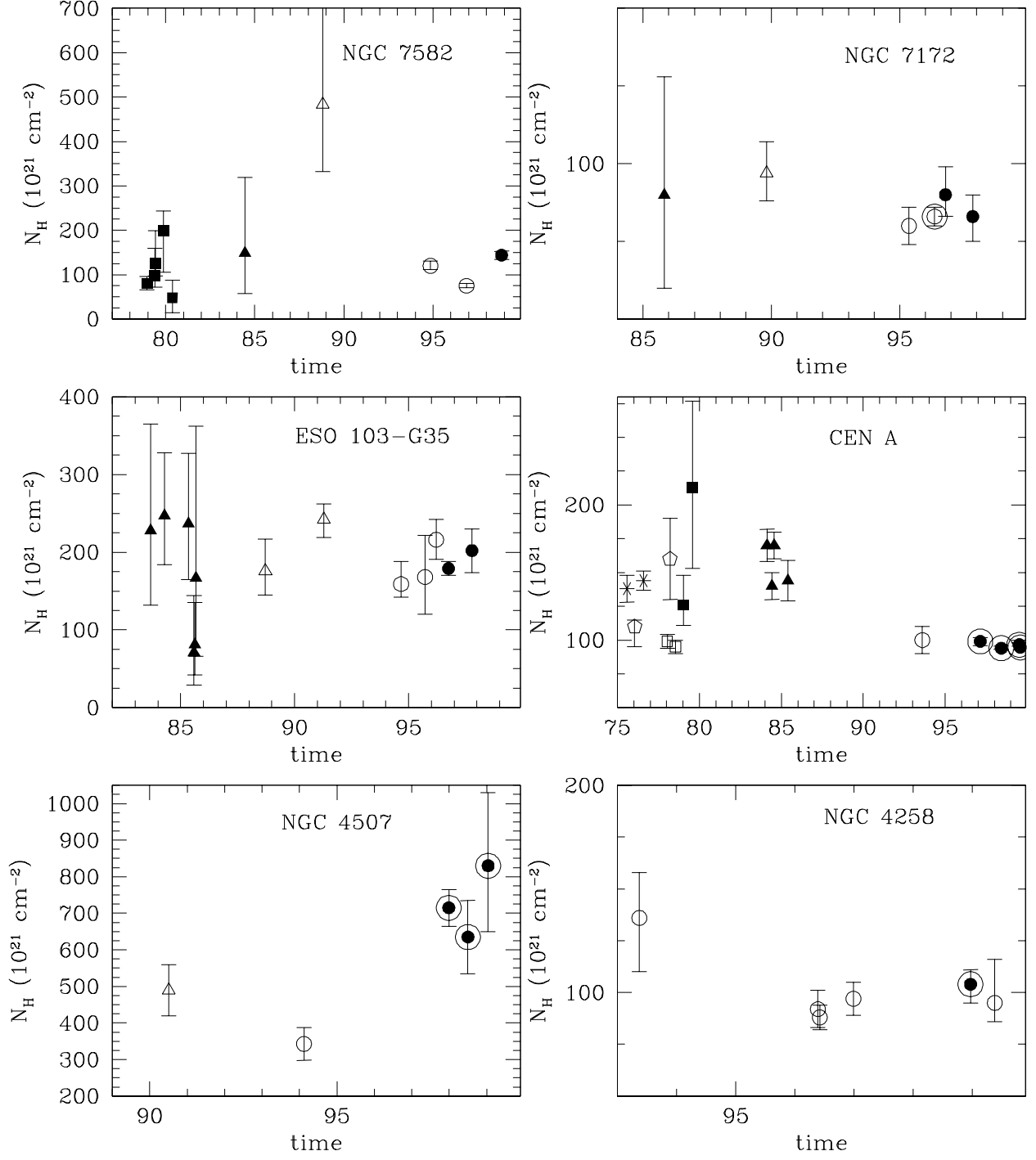
Fig. 6.— Distance from the center (in units of  $R_S$ ) versus cloud density. The box on the upper-left of the diagram is the region of the parameter space occupied by a standard parsec-scale torus. The box on the bottom-right represents the BELR. The three lines are obtained from Equations 3, 6 and 7. The shortest variations observed, with timescales of a few months, rule out the parsec-scale torus scenario. Instead, timescales of  $\sim 1$  day are in agreement with the hypothesis of an absorber located in the BELR.

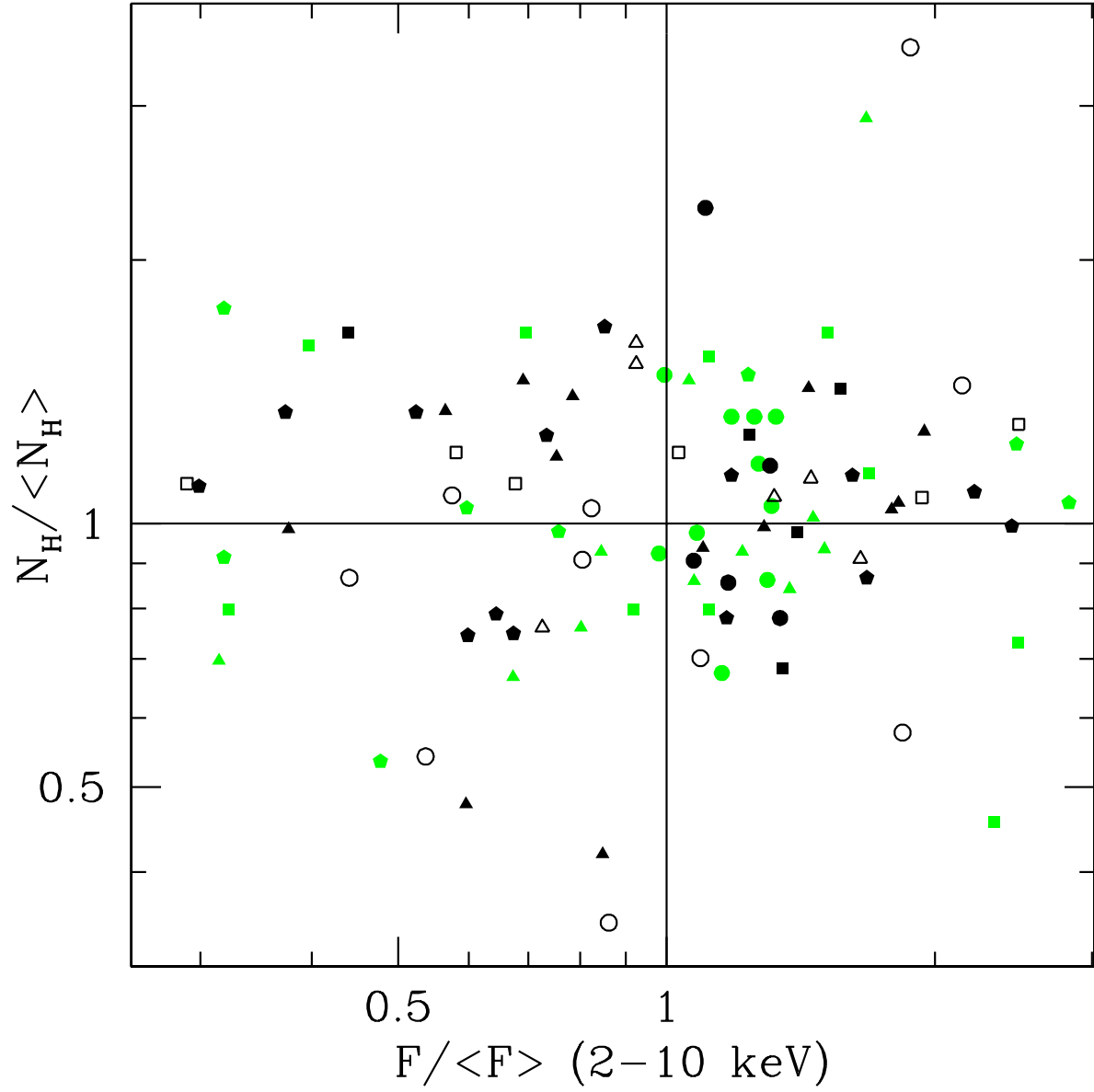
Fig. 7.— Column density distribution for the single absorbing clouds, estimated as the ratio of the average  $N_H$  and the expected number of clouds,  $N_C$ , along the line of sight.

Fig. 8.— A simple model, derived from Elvis (2000) to explain Seyfert 2 X-ray absorption properties. Both broad emission lines (emitted by the inner clouds) and the X-ray continuum (emitted by the central region of the accretion disk) are absorbed by the clouds inside the wind. The column density variability timescale is the average crossing time of a cloud along the line of sight. Note that the dimensions are different from the original Elvis 2000 model, where the radial size of the wind is  $\sim 10^{16} \text{ cm}$  (see text for details).

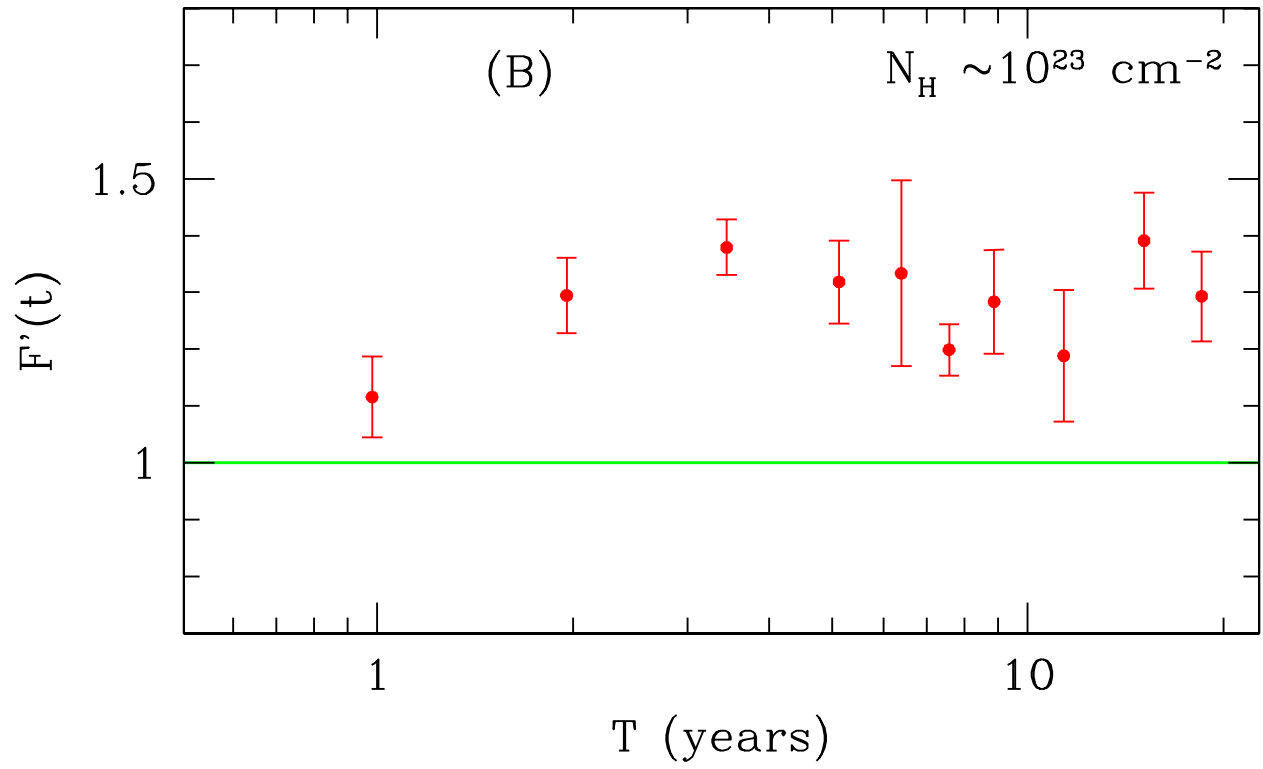
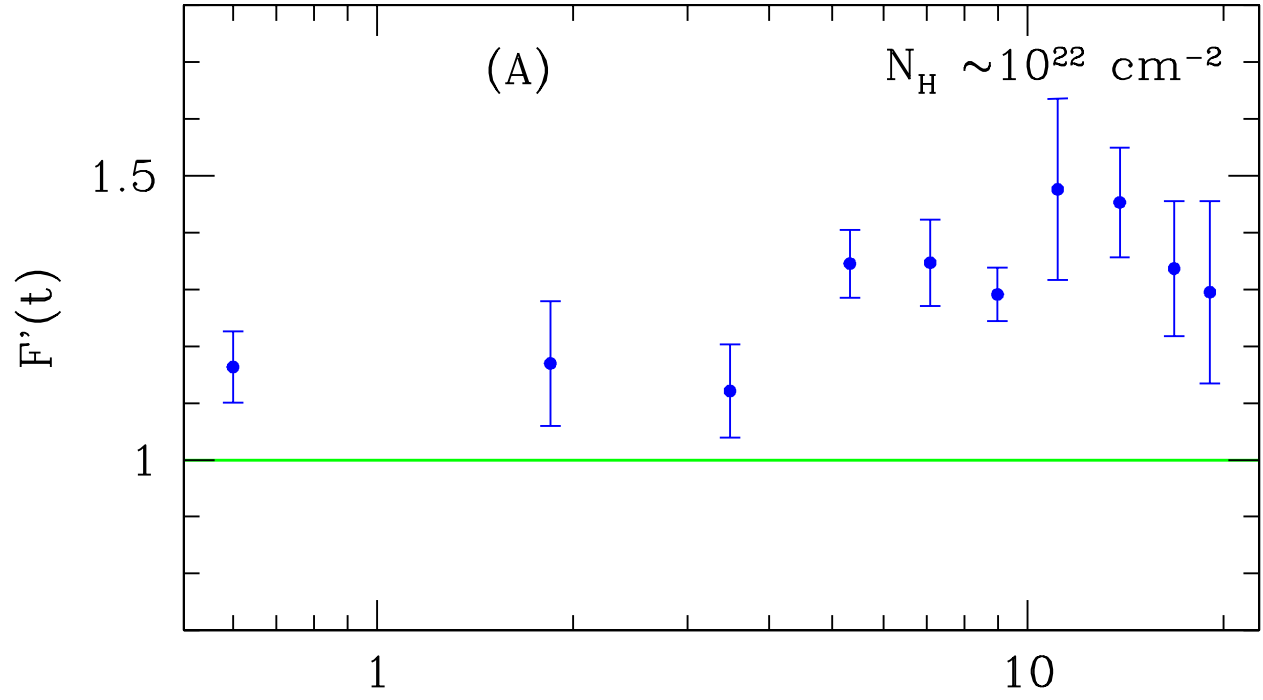


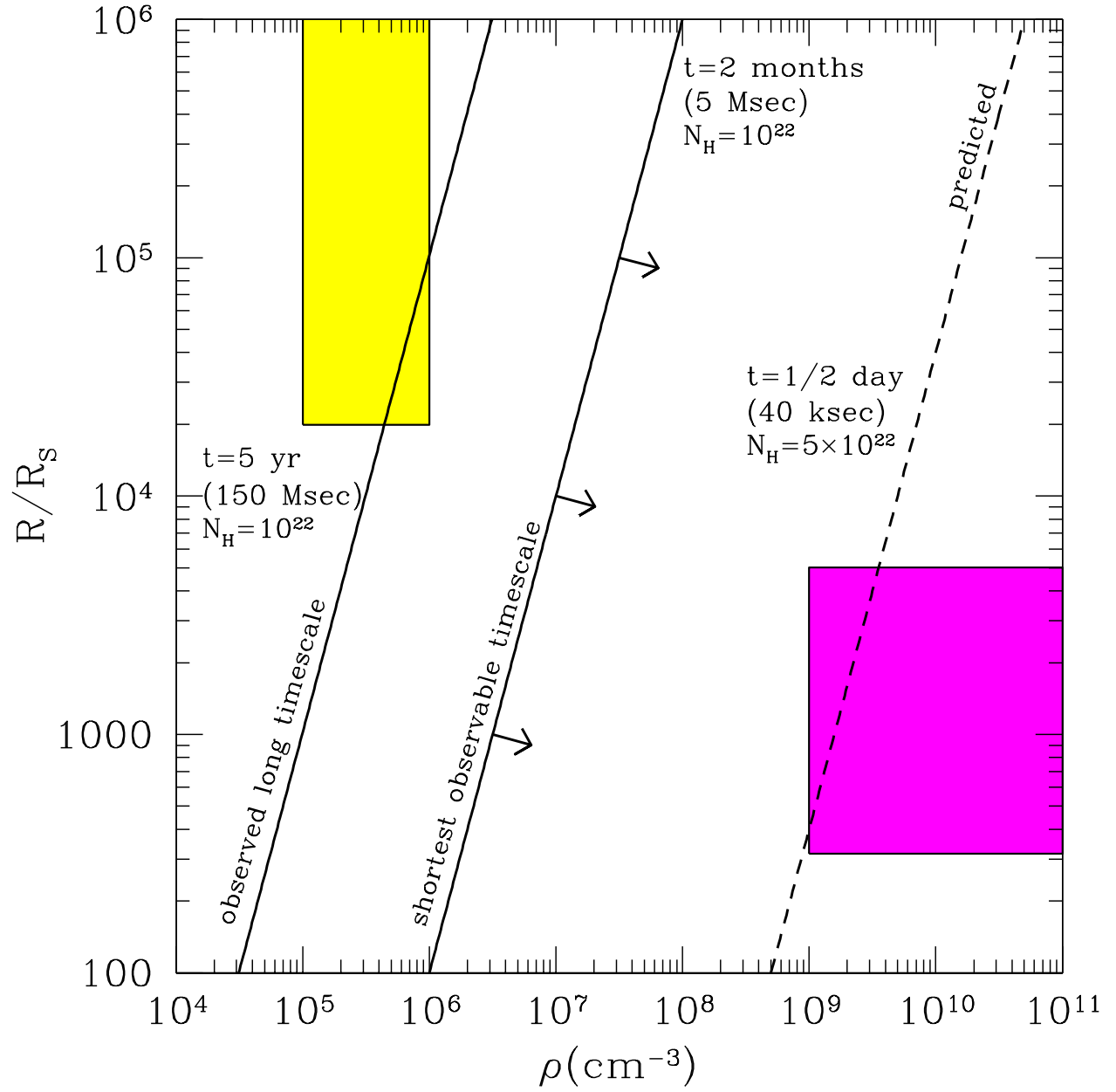


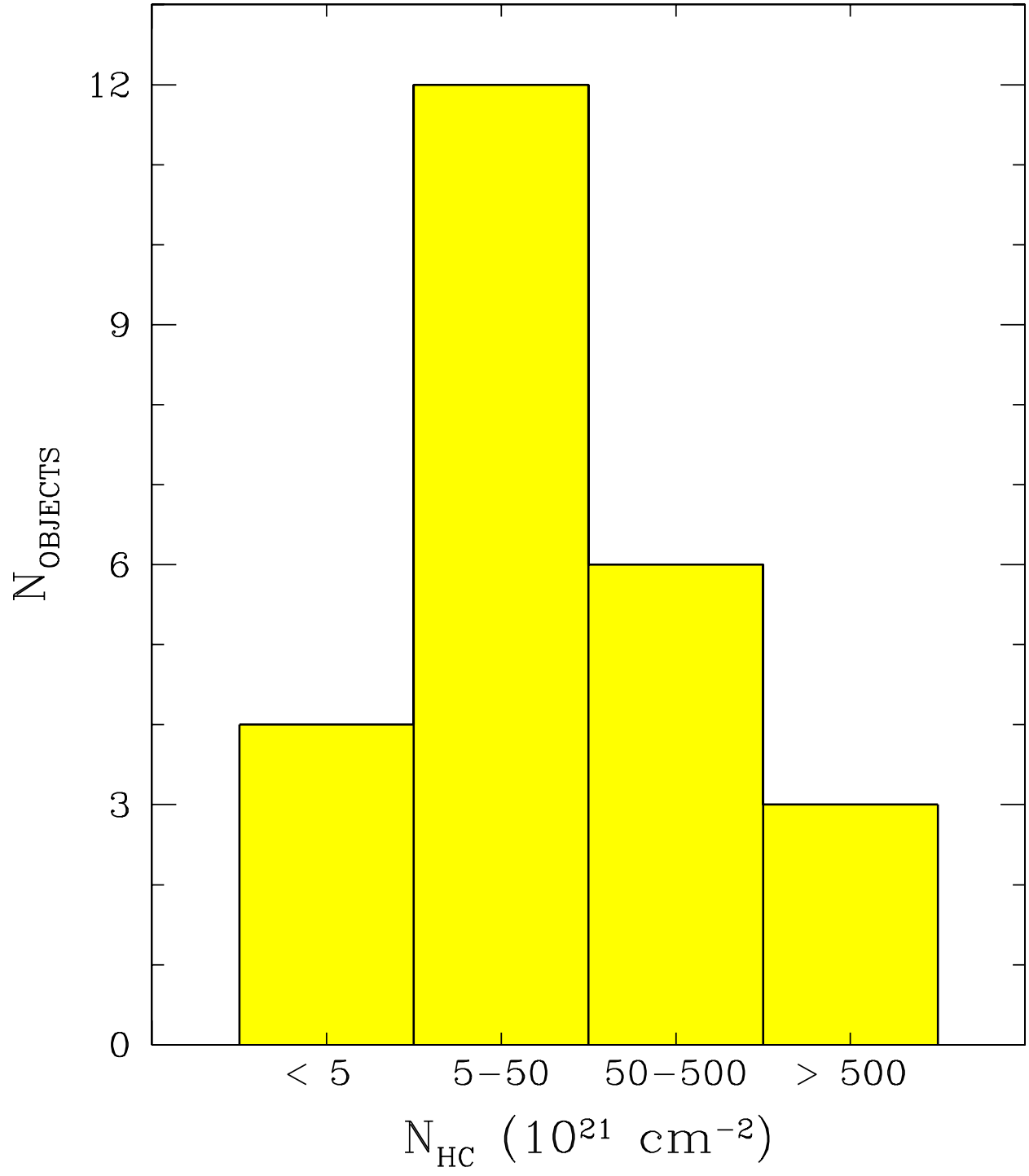












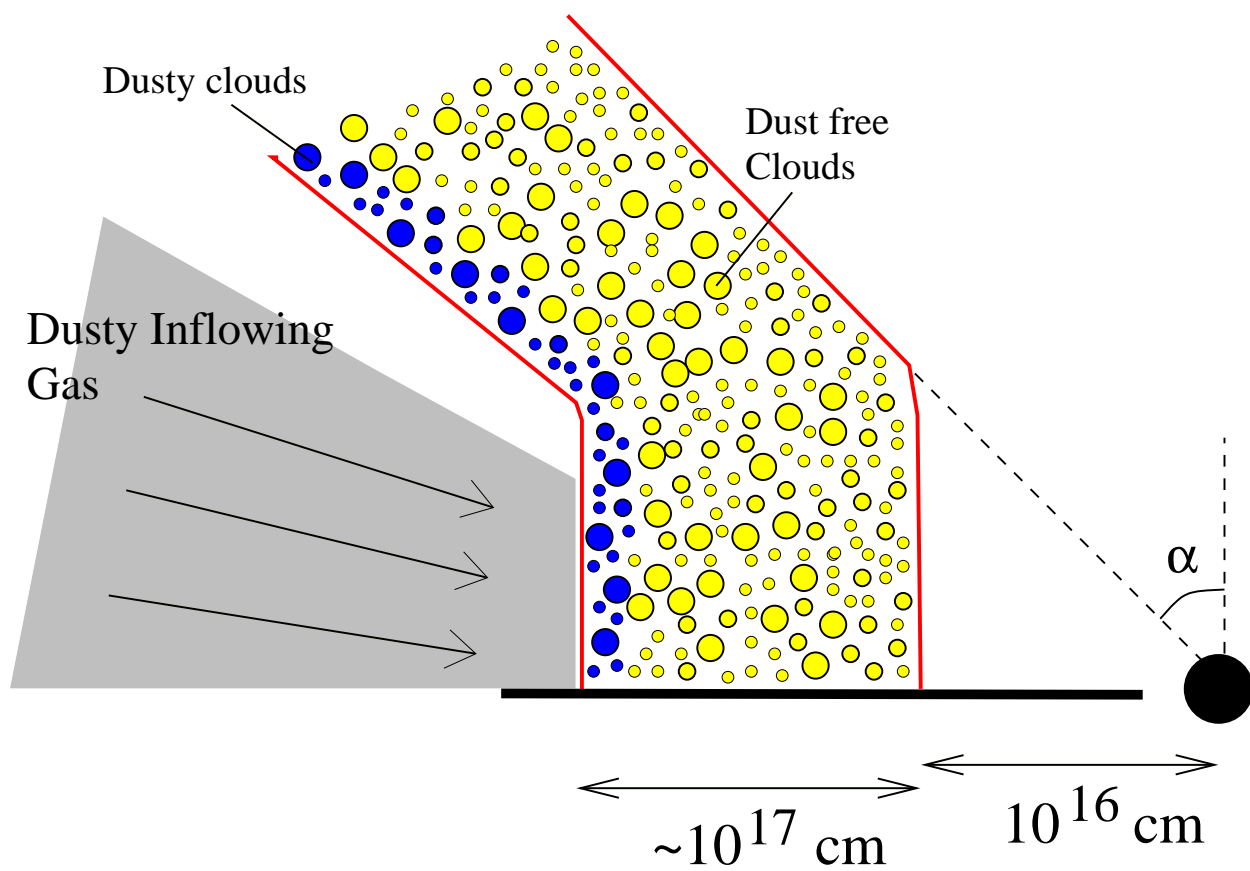


Table 1. Data for our sample of Seyfert 2s

#	Name	Obs. date	Instrument	$N_H^a$	$F(2-10 \text{ keV})^b$	Ref.
1	MKN 348	13.06.1987	GINGA	$106^{+31}_{-26}$	2.2	2
	Sy 2	04.08.1995	ASCA	$160^{+20}_{-10}$	0.8	24
2	NGC 526a <sup>(A)</sup>	23.05.1978	HEAO 1	$15^{+15}_{-13}$	1.5	6
	Sy 2/1.5	09.12.1978	HEAO 2	$17.5^{+6}_{-7}$	6.2	9
		05.08.1983	EXOSAT	$21^{+11}_{-9}$	3.1	3
		28.06.1985	EXOSAT	$13^{+42}_{-5}$	0.8	3
		23.08.1985	EXOSAT	$25^{+53}_{-12}$	0.8	3
		15.12.1988	GINGA	$7.6^{+6}_{-6}$	1.2	2
		30.11.1995	ASCA	$15^{+1.4}_{-1.4}$	7.1	4
		01.01.1999	SAX	$16^{+2}_{-2}$	1.9	1
3	NGC 1365	25.01.1995	ASCA	$> 10000$	–	12
	Sy 1.8	12.08.1997	SAX	$400^{+40}_{-50}$	2.1	13
4	NGC 1386	26.01.1995	ASCA	$280^{+270}_{-260}$	0.065	12
	Sy 2	10.12.1996	SAX	$> 1000$	–	22
5	IRAS 04575-7537	04.10.1990	GINGA	$12.3^{+7}_{-4}$	1.6	2
	Sy 2	04.11.1996	ASCA	$10.5^{+1}_{-1}$	2.0	23
6	NGC 1808	15.10.1990	GINGA	$105^{+1.4}_{-1.4}$	0.3	25
	Sy 2	26.02.1994	ASCA	$< 2.5$	0.09	4
7	IRAS 05189-2524	15.02.1995	ASCA	$44^{+4}_{-4}$	0.6	10
	Sy 2	03.10.1999	SAX	$85^{+8}_{-8}$	0.7	10
8	NGC 2110 <sup>(A)</sup>	09.10.1978	HEAO1	$67^{+11}_{-11}$	3.3	6
	Sy 2	26.09.1989	GINGA	$22.8^{+2}_{-2}$	4.0	2
		06.12.1990	BBRXT	$25^{+5}_{-5}$	3.5	7
		12.03.1990	ASCA	$26.5^{+2}_{-1.6}$	3.2	4
		14.10.1997	SAX	$34^{+3}_{-3}$	3.9	8
9	NGC 2992 <sup>(A)</sup>	24.05.1978	HEAO 1	$4.0^{+0.8}_{-4}$	9.4	32
	Sy 1.9	22.11.1978	HEAO 2	$6.4^{+2.7}_{-2.8}$	10.0	9
		02.06.1979	HEAO 2	$14.5^{+10}_{-6}$	2.8	9
		06.06.1980	HEAO 2	$10^{+3}_{-4.5}$	6.8	9
		09.06.1980	HEAO 2	$14.5^{+6.3}_{-5.4}$	6.1	9
		18.12.1983	EXOSAT	$7^{+6}_{-1.4}$	1.3	9

Table 1—Continued

#	Name	Obs. date	Instrument	$N_H^a$	$F(2-10 \text{ keV})^b$	Ref.
10	MCG-5-23-16 <sup>(A)</sup> Sy 2	06.04.1984	EXOSAT	$7.8^{+14}_{-1.9}$	4.5	9
		09.11.1984	EXOSAT	$7^{+3}_{-0.3}$	3.7	3
		30.04.1990	GINGA	$16.1^{+4}_{-7}$	1.57	2
		30.06.1996	ASCA	$7^{+3}_{-2}$	0.35	4
		30.11.1997	SAX	$14^{+5}_{-4}$	0.7	14
		30.11.1998	SAX	$9^{+0.3}_{-0.3}$	7.8	14
		12.05.1978	HEAO 1	$50^{+20}_{-20}$	11.7	6
		23.06.1979	HEAO 2	$18^{+3}_{-7}$	10.2	9
		31.12.1980	HEAO 2	$14.5^{+5}_{-4}$	9.6	9
		04.01.1981	HEAO 2	$25^{+6}_{-3}$	7.4	9
		13.12.1983	EXOSAT	$15^{+4}_{-4}$	7.5	3
		23.04.1984	EXOSAT	$16^{+4}_{-4}$	5.9	3
		30.11.1988	GINGA	$19.4^{+4}_{-5}$	4.7	2
		05.12.1988	GINGA	$18.1^{+4}_{-8}$	2.2	2
		27.11.1991	ROSAT	$13.1^{+1.6}_{-1.3}$	5.6	15
11	NGC 3081 Sy 2	11.05.1994	ASCA	$16^{+0.5}_{-0.7}$	8.5	4
		25.04.1998	SAX	$15.9^{+0.4}_{-0.4}$	10.5	1
		13.05.1996	ASCA	$500^{+140}_{-120}$	2.6	1
12	NGC 4258 <sup>(B)</sup> Sy 1.9	20.12.1996	SAX	$640^{+200}_{-120}$	0.8	22
		15.05.1993	ASCA	$136^{+22}_{-26}$	1.4	34
		23.05.1996	ASCA	$92^{+9}_{-9}$	2.0	34
13	NGC 4388 Sy 2	06.06.1996	ASCA	$88^{+7}_{-6}$	2.2	34
		28.12.1996	ASCA	$97^{+8}_{-8}$	2.5	34
		19.12.1998	SAX	$121^{+7}_{-6}$	1.4	1
		17.05.1999	ASCA	$95^{+21}_{-9}$	1.1	34
		04.07.1993	ASCA	$315^{+110}_{-100}$	3.2	20
		21.06.1995	ASCA	$334^{+100}_{-90}$	1.5	20
		09.01.1999	SAX	$380^{+20}_{-40}$	8.2	1
14	NGC 4507 <sup>(B)</sup> Sy 2	03.01.2000	SAX	$480^{+180}_{-80}$	2.8	1
		07.07.1990	GINGA	$490^{+70}_{-70}$	5.1	2
		12.02.1994	ASCA	$343^{+45}_{-45}$	4.9	4

Table 1—Continued

#	Name	Obs. date	Instrument	$N_H^a$	$F(2-10 \text{ keV})^b$	Ref.
15	NGC 4941	09.04.1997	SAX	$590^{+80}_{-120}$	5.7	1
		19.02.1998	SAX	$540^{+90}_{-70}$	4.5	1
		04.01.1999	SAX	$710^{+20}_{-160}$	1.6	1
		19.07.1996	ASCA	$> 1000$	–	1
	Sy 2	22.01.1997	SAX	$450^{+250}_{-140}$	0.3	22
16	IRAS 13197-164	18.07.1995	ASCA	$760^{+130}_{-120}$	0.6	11
	Sy 1.8	22.07.1998	SAX	$330^{+50}_{-40}$	1.9	1
17	CENTAURUSA <sup>(B)</sup>	27.07.1975	OSO 8	$139^{+9}_{-9}$	148	27
	Sy 2	19.01.1976	ARIEL 5	$110^{+5}_{-15}$	112	28
		01.08.1976	OSO 8	$144^{+7}_{-7}$	79	27
		15.01.1978	HEAO 1	$99^{+5}_{-5}$	78	29
		15.03.1978	ARIEL 5	$160^{+30}_{-30}$	49	28
		15.07.1978	HEAO 1	$95^{+5}_{-5}$	45	29
		15.01.1979	HEAO 2	$126^{+22}_{-15}$	163	9
		03.08.1979	HEAO 2	$213^{+64}_{-60}$	57	9
		13.02.1984	EXOSAT	$164^{+8}_{-8}$	35	30
		08.06.1984	EXOSAT	$140^{+10}_{-10}$	20	30
		30.07.1984	EXOSAT	$170^{+10}_{-10}$	25	30
		29.05.1985	EXOSAT	$144^{+1.5}_{-1.5}$	108	30
		14.08.1993	ASCA	$100^{+10}_{-10}$	43	31
		20.02.1997	SAX	$100^{+3}_{-2}$	34	1
		06.01.1998	SAX	$93.0^{+1.3}_{-1.7}$	43	1
		10.07.1999	SAX	$94.3^{+2.3}_{-0.8}$	40	1
		02.08.1999	SAX	$93.6^{+1.7}_{-1.8}$	40	1
		08.01.2000	SAX	$94.3^{+1.4}_{-1.1}$	39	1
18	NGC 5252	28.01.1994	ASCA	$43^{+7}_{-6}$	0.75	4
	Sy 1.9	20.01.1998	SAX	$68^{+16}_{-7}$	3.8	1
19	NGC 5506 <sup>(A)</sup>	20.01.1978	HEAO 1	$41^{+22}_{-18}$	6.8	6
	Sy 1.9	13.07.1979	HEAO 2	$38^{+7}_{-7}$	8.8	9
		21.07.1979	HEAO 2	$48^{+25}_{-14}$	6.9	9
		30.07.1979	HEAO 2	$43^{+10}_{-12}$	8.7	9

Table 1—Continued

#	Name	Obs. date	Instrument	$N_H^a$	$F(2-10 \text{ keV})^b$	Ref.
20	IRAS 18325-5926 Sy 1.8	09.08.1979	HEAO 2	$43_{-7}^{+8}$	9.2	9
		06.01.1981	HEAO 2	$43_{-12}^{+5}$	8.2	9
		24.01.1986	EXOSAT	$28_{-5}^{+5}$	9.0	3
		19.07.1988	GINGA	$29_{-2}^{+3}$	1.0	2
		06.01.1992	ROSAT	$21.9_{-2.4}^{+2.6}$	8.0	15
		30.01.1997	SAX	$37_{-1}^{+2}$	7.5	1
		14.01.1998	SAX	$39_{-2}^{+1}$	9.1	1
		13.05.1989	GINGA	$16.3_{-2.6}^{+7}$	12.8	2
		11.09.1993	ASCA	$13.2_{-1}^{+1}$	1	26
		27.03.1997	ASCA	$10.4_{-0.4}^{+0.4}$	2.5	1
21	ESO 103-G35 <sup>(B)</sup> Sy 2	04.09.1983	EXOSAT	$228_{-98}^{+137}$	1.8	18
		19.04.1984	EXOSAT	$247_{-63}^{+81}$	2.2	18
		04.05.1985	EXOSAT	$237_{-72}^{+90}$	2.5	18
		02.08.1985	EXOSAT	$71_{-42}^{+73}$	2.7	18
		13.08.1985	EXOSAT	$81_{-39}^{+54}$	1.9	18
		04.09.1985	EXOSAT	$167_{-101}^{+195}$	1.2	18
		23.09.1988	GINGA	$176_{31}^{+41}$	5.7	19
		12.04.1991	GINGA	$292_{-24}^{+25}$	4.6	2
		03.09.1994	ASCA	$216_{-35}^{+40}$	3.5	20
		26.09.1995	ASCA	$168_{-48}^{+54}$	4.1	20
		18.03.1996	ASCA	$216_{-25}^{+26}$	6.2	20
		03.10.1996	SAX	$179_{-9}^{+9}$	5.8	21
		14.10.1997	SAX	$202_{-28}^{+28}$	2.4	21
		02.10.1990	GINGA	$252_{-78}^{+95}$	2.3	2
		25.04.1994	ASCA	$256_{-70}^{+89}$	2.6	4
22	IC 5063 Sy 2	27.04.1994	ASCA	$218_{-21}^{+22}$	2.7	4
		26.10.1989	GINGA	$112_{-8}^{+7}$	7.7	2
		28.10.1985	EXOSAT	$90_{-30}^{+38}$	3.2	3
		11.05.1995	ASCA	$82_{-4}^{+4}$	6.0	4
		17.05.1996	ASCA	$77_{-7}^{+8}$	2.1	1
		14.10.1996	SAX	$90_{-7}^{+9}$	1.8	5



Table 1—Continued

#	Name	Obs. date	Instrument	$N_H^a$	$F(2-10 \text{ keV})^b$	Ref.
24	NGC 7314 Sy 1.9	06.11.1997	SAX	$83^{+5}_{-5}$	0.9	5
		05.09.1983	EXOSAT	$13^{+35}_{-4}$	1.3	3
		25.03.1984	EXOSAT	$8.2^{+8.9}_{-0.9}$	3.2	3
		20.11.1994	ASCA	$8.9^{+0.4}_{-1.0}$	3.6	4
25	NGC 7582 <sup>(B)</sup> Sy 2	08.06.1999	SAX	$12.2^{+0.2}_{-1.4}$	2.6	1
		14.12.1978	HEAO 2	$80^{+16}_{-14}$	9.6	9
		26.05.1979	HEAO 2	$97^{+62}_{-25}$	5.7	9
		02.06.1979	HEAO 2	$126^{+73}_{-29}$	4.2	9
		21.11.1979	HEAO 2	$199^{+45}_{-93}$	11.2	9
		15.05.1980	HEAO 2	$48^{+39}_{-34}$	4.5	9
		09.06.1984	EXOSAT	$149^{+170}_{-91}$	3.0	16
		25.10.1988	GINGA	$484^{+254}_{-152}$	9.8	19
		14.11.1994	ASCA	$120^{+11}_{-8}$	2.3	33
		21.11.1996	ASCA	$75^{+5}_{-4}$	2.8	33
		10.11.1998	SAX	$144^{+9}_{-10}$	4.3	17

<sup>a</sup>X-ray absorbing column density, in units of  $10^{21} \text{ cm}^{-2}$

<sup>b</sup>2-10 keV intrinsic flux, in units of  $10^{-11} \text{ erg s}^{-1} \text{ cm}^{-2}$

References. — (1) This work (2) Smith & Done 1996; (3) Turner & Pounds 1989; (4) Turner et al. 1997; (5) Akylas et al. 2001; (6) Weaver et al. 1995; (7) Weaver 1993; (8) Malaguti et al. 1999; (9) Halpern 1981; (10) Severgnini et al. 2000; (11) Bassani et al. 1999; (12) Iyomoto 1997; (13) Risaliti et al. 2000; (14) Gilli et al. 2000; (15) Mulchaey et al. 1993; (16) Malaguti et al. 1994; (17) Turner et al. 2000; (18) Warwick et al. 1988; (19) Warwick et al. 1993; (20) Forster et al. 1999; (21) Wilkes et al. 2000; (22) Maiolino et al. 1998; (23) Vignali et al. 1998; (24) Awaki et al. 2000; (25) Awaki & Koyama 1993 (26) Iwasawa et al. 1996; (27) Mushotzky et al. 1978; (28) Stark (1979); (29) Baity et al. 1981; (30) Morini et al. 1989; (31) Sambruna et al. 1999; (32) Singh et al. 1985; (33) Xue et al. 1999.; (34) Reynolds et al. 2000

Table 2. Fastest  $N_H$  variations.

Name	Time interval <sup>a</sup>	variation (%) <sup>b</sup>	# Obs.	$N_{HC}$ <sup>c</sup>
CENTAURUS A	2 months	46%	18	2.3
NGC 4258	5 months	10%	6	1.6
NGC 2110	6 months	15%	5	2.2
NGC 4941	6 months	> 81%	2	27.5
NGC 7582	6 months	122%	10	3.5
NGC 2992	6.5 months	40%	12	0.4
ESO 103-G35	6.5 months	19%	13	5.5
NGC 4507	11 months	25%	5	19
NGC 4388	1 year	50%	4	16.5
MCG-5-23-16	1.1 years	94%	11	0.6
NGC 1386	2 years	>112%	2	36
NGC 1365	2.5 years	> 85%	2	30
IRAS 13197-164	3 years	44%	2	22
NGC 1808	3.3 years	200%	2	45
NGC 5506	3.5 years	28%	11	1.1
IRAS 18325-5926	3.5 years	24%	3	0.2
NGC 7172	3.5 years	31%	6	1.5
NGC 5252	4 years	36%	2	1.3
NGC 7314	4.5 years	31%	4	0.2
IRAS 05189-2524	4.6 years	64%	2	2.0
NGC 256a	5 years	94%	8	0.4
MKN 348	8 years	20%	2	2.5
IRAS 04575-7537	–	–	2	–
NGC 3081	–	–	2	–
IC 5063	–	–	3	–

<sup>a</sup>Time interval between the two closest variations of  $N_H$  statistically significant at > 90%.

<sup>b</sup>Variation with respect to the average  $N_H$ , calculated using the best fit values in Table 1.

<sup>c</sup>Estimated  $N_H$  of a single cloud, in units of  $10^{22} \text{ cm}^{-2}$  (see text for details).